European Polymer Journal 122 (2020) 109338

Contents lists available at ScienceDirect

European Polymer Journal

journal homepage: www.elsevier.com/locate/europolj

Facile green synthesis of bioresorbable polyester from soybean oil and recycled plastic waste for osteochondral tissue regeneration

Krishanu Ghosal, Upama Bhattacharjee, Kishor Sarkar*

Gene Therapy and Tissue Engineering Lab, Department of Polymer Science and Technology, University of Calcutta, 92, A.P.C. Road, Kolkata 700009, India

ARTICLE INFO

Keywords:
Polyester
Polyethylene terephthalate waste
Soybean oil
Osteochondral tissue
Interfacial tissue engineering

ABSTRACT

Despite the recent progress in the field of tissue engineering still there are great challenges to regenerate osteochondral tissue interface due to its complex material composition and mechanical properties. A series of biomaterials have been developed in the last few decades, still suitable biomaterial remained undiscover to regenerate osteochondral tissue interface. Here we have reported a new family of low cost biopolymer derived from edible soybean oil (SO) and recycled polyethylene terephthalate (PET) waste along with other renewable resources such as citric acid, sebacic acid and mannitol by facile catalyst and solvent free melt polycondensation process. The physicochemical properties of the synthesized polyester can be tailored by simply varying the monomer feed ratio. The polyesters were found to be elastomeric and biodegradable in nature. 3D porous scaffold shows *in vitro* mineralization which attributes that the polymer may be applicable for bone formation. 2D polyester film exhibited excellent cytocompatibility to the stem cell and interestingly the polyester guided the stem cell towards both osteogenic and chondrogenic differentiation without using any external differentiating chemicals. Thus this novel class of polyester derived from SO, recycled PET waste and other low cost renewable resources may be a potential candidate in field of interfacial tissue engineering for the treatment of arthritic patients in future.

1. Introduction

Osteoarthritis (OA) is the most common type of joint disorder by which the articular cartilage and subchondral bone are damaged and subsequently results severe pain, inflammation and inadequate quality of life. Presently, more than 250 million of people are suffering from OA throughout the world which is a serious impact on health care and society [1,2]. Currently there is no therapeutic treatment to cure OA or to regenerate the damaged tissues such as cartilage and subchondral bone. Although, knee replacement, joint replacement, periosteal grafts, lavage and mosaicplasty are the only available surgical procedure to relive the disability from OA [3–7]. But, degenerative alteration and immune rejection limit its long term therapeutic effect [8,9]. So researchers and clinicians are looking for alternative way to repair osteochondral defect.

Over the past few decades, tissue engineering has shown great promise to regenerate damaged tissues or organs due to accident, trauma and life threatening diseases [10–13]. Successful tissue engineering comprises 3D porous scaffold (acts as extracellular matrix (ECM) for cell attachment, proliferation and differentiation), cells and cell signaling molecules such as growth factors [14–17]. For successful tissue engineering an ideal scaffold should be biocompatible, biodegradable and highly porous interconnected structure with sufficient physical and mechanical properties [14,18]. However, conventional tissue engineering using polymeric scaffolds are capable to regenerate functional tissues like cartilage, bone, skin, tendon, ligament, etc. [19–23] but unable to regenerate interfacial osteochondral tissues such as bone-cartilage, ligament-bone etc. due to presence of complex chemical composition and mechanical properties [24–29]. The self-renewal incapability of articular cartilage demands new biomaterial or tissue engineering approach for the regeneration of osteochondral tissue. In this regard, interfacial tissue engineering (ITE) has gained tremendous attention due to its capability to regenerate interfacial osteochondral tissue [7,30–32]. Despite the development of a series of biomaterials from ceramic to inorganic to polymeric materials, there is no single biomaterial which is capable to regenerate osteochondral tissue. Some strategies reported for osteochondral tissue regeneration including bilayered [33–35], multilayered [36–39], and gradient scaffold fabrication [32,40–42]. In most of the work, either some signaling molecules such as hydroxyl apatite, bone morphogenic protein-2 (BMP-

* Corresponding author.
E-mail address: kspoly@caluniv.ac.in (K. Sarkar).
URL: http://www.kishorgttl.com (K. Sarkar).

https://doi.org/10.1016/j.eurpolymj.2019.109338
Received 13 September 2019; Received in revised form 22 October 2019; Accepted 24 October 2019
Available online 31 October 2019

2), tumor growth factor-β (TGF-β), insulin growth factor (IGF) etc. or physical stimulus like mechanical properties, structural pattern etc. are used separately or in combination both to regenerate for bone and cartilage, respectively. Due to short half-life and huge cost of growth factors restrict its clinical translation. Apart from this, polycaprolactone (PCL), polyethylene glycol (PEG), polylactide-co-glycolide (PLGA), chitosan, collagen, gelatin etc. have been used extensively for scaffold fabrication. But, improper mechanical property, longer degradation time, high cost, complicated synthesis procedure, immunogenic problem are the major drawbacks of the existing polymeric materials. Hence, there is a big demand of biopolymers having low cost, ease of synthesis, tunable mechanical properties and limited degradation time for ITE application.

Over the last few decade, the use of PET has increased enormously due to its extensive applications in food and packaging industry and resulted in an increasing volume of industrial and post-consumer PET waste. Thus recycling and reuse of PET waste has become a significant challenge throughout the globe [43,44]. Till now various processes such as glycolysis [45], aminolysis [46,47] and methanolysis [48] have been used extensively for recycling of PET waste. Among these, glycolysis is economically more favorable over other chemical recycling processes [49]. In this context, Sarkar et al. [50] recently developed biodegradable polyester for bone tissue engineering application by using PET glycolysis mediated BHET (bis(2-Hydroxyethyl) terephthalate) as a starting material along with other renewable resourced monomers. In another study, they also developed soybean oil (SO) based polyester which showed osteogenic differentiation of human mesenchymal stem cell (hMSC) even in absence of any osteogenic compound [51]. Being inspired from these works, it was hypothesized that the combination of BHET and SO based polymer may be an interesting novel biopolymer for ITE application due to inclusion of hard and soft segments by BHET and SO, respectively in polymer backbone.

In this work, BHET and SO based polyol was synthesized by reacting of BHET and epoxidized SO (ESO). The polyol of BHET and SO was then polymerized by catalyst and solvent free melt polycondensation reaction with other renewable resourced monomers such as sebacic acid (SA), citric acid (CA) and mannitol (MA) which are well known biocompatible and inexpensive monomers [52–54].

The mechanical, thermal and degradation properties of the polymer was dependent on BHET and SO weight ratios. Interestingly, the polymer showed both osteogenesis and chrondogenesis of mouse embryonic stem cell (OP9) without using any differentiating compounds such as bone morphogenetic protein-2 (BMP-2) or tumor growth factor-β3 (TGF-β3). Therefore, the BHET-SO based polyester may be an interesting low cost biopolymer for ITE application.

2. Experimental section

2.1. Materials

PET bottles were purchased from Milton India. Soybean oil was purchased from local market at Kolkata and manufactured by Ruchi Soya Industries Limited (India). Ethylene glycol, alizarin red S, alcian blue and guanidine hydrochloride were obtained from Sisco Research Laboratories Pvt. Ltd. (India). Glacial formic acid, sulfuric acid (98%), hydrogen peroxide (30%), citric acid, mannitol, sodium chloride, sodium bicarbonate ($NaHCO_3$), potassium chloride, potassium hydrogen phosphate trihydrate, magnesium chloride hexahydrate, hydrochloric acid (37%), calcium chloride, sodium sulphate and ethanol were purchased from Merck India. Sebacic acid was obtained from LobaChemie. Acetone-D_6 was purchased from Chembridge Isotope Laboratories. Chloroform-D, and (3-(4,5-dimethylthiazol-2-yl)-2,5-diphenyltetrazolium bromide) (MTT) were bought from Sigma Aldrich. Dulbecco's modified eagle's media (DMEM), fetal bovine serum (FBS), penicillin–streptomycin, trypsin–EDTA, Dulbecco's phosphate-buffered saline (DPBS) and molecular grade water were obtained from HiMedia Laboratories Pvt. Ltd (India). All other chemicals were analytical grade and used as received.

2.2. Synthesis of BHET, ESO and EBHET-OH (polyol)

BHET was synthesized by depolymerization of PET as reported earlier with minor modifications [50]. Briefly, 100 g of washed PET flakes with $5 \times 5\ mm^2$ dimension, 333 g of ethylene glycol and 1.0 g of zinc acetate as a catalyst were charged into a three necked 1000 ml round bottom flask equipped with a magnetic stirrer, a reflux condenser and a thermometer was put on an oil bath. After degassing of the flask with nitrogen gas for 30 min, the temperature of the oil bath was raised to 198 °C and the reaction was carried out under nitrogen atmosphere at 198 °C for 8 h with constant stirring. The reaction temperature was then cooled down to room temperature and the crude product was collected by addition of 1000 ml of distilled water followed by filtering with Buchner funnel. The solid cake was re-suspended in 1000 ml distilled water and boiled for 30 min to dissolve the BHET due to its insolubility in water at room temperature. After filtering the solution in hot condition, the supernatant was cooled down to room temperature followed and kept the solution at 4 °C overnight. The purified BHET crystals were obtained after the filtration of chilled solution followed by drying the BHET crystals at 60 °C for 24 h (yield: ~60%).

Epoxidized soybean oil (ESO) was synthesized according to the previous report with slight changes [51]. In details, 200 ml of SO and 22 ml of glacial formic acid were taken in to 500 ml round bottom flask and placed in an oil bath at 55° C followed by addition of 1 ml of concentrated sulfuric acid with continuous stirring. After that, 162 ml of 30% hydrogen peroxide was added drop wise over a period of 1 h to avoid the increment of temperature as it is highly exothermic reaction and the reaction was continued for another 7 h at 55 °C. After completion of the reaction, the crude product was filtered to separate out excess water followed by washing with water for several times till it becomes to neutral pH. Finally, the light yellowish colored ESO was obtained by rotary evaporation followed by vacuum drying at 60 °C for 24 h.

EBHET-OH (polyol) was synthesized by the ring opening reaction of ESO by BHET at different ESO and BHET weight ratios such as 3:1, 4:1, 5:1 and 6:1. The reaction was carried out in a two necked round bottom flak equipped with constant stirring at 160 °C under nitrogen atmosphere for 7 h. The synthesized EBHET-OH was used directly for the synthesis of all polyesters.

2.3. Synthesis of polyester

The polyester was synthesized through melt polycondensation reaction by reacting EBHET-OH and other renewable resourced monomers such as SA, CA and MA. The synthesis of polyester was consisted of two successive steps including pre-polymerization and post-polymerization. Pre-polymerization was carried out by reacting 4 g of EBHET-OH, 2 g of SA and 2 g of CA in a two neck round bottom flask and placed in an oil bath at 160 °C with constant nitrogen gas purging. After 1.5 h of the reaction, 1 g of MA was added to the reaction mixture and reacted for another 30 min. The reaction was stopped by cooling down the temperature to room temperature and a brown colored waxy pre-polymer was obtained. A series of polyesters was synthesized by using the various EBHET polyols of different weight ratios (3:1, 4:1, 5:1 and 6:1) with keeping constant the final weight ratio of EBHET-OH: SA: CA: MA at 2: 1: 1: 0.5. The pre-polymer was then transferred to Teflon petri dish and kept it in an oven at 120 °C for post-polymerization. After 5 day of post-polymerization, deep brown colored polyester was obtained and used for all experiments.

2.4. Characterization of polyester

Prior the characterization, the pre-polymer was purified by washing

with double distilled water to remove unreacted monomers MA and CA and then with hot water to eliminate unreacted BHET. After that, the pre-polymer was dissolved in acetone and re-precipitated in water/isopropanol mixture to separate out unreacted SA. The purified pre-polymer was collected after repeating the solution precipitation method thrice followed by drying overnight at 60 °C in vacuum oven.

The synthesized ESO, BHET, EBHET-OH and polyesters were characterized by Fourier transform infrared spectrophotometer (FTIR) equipped with attenuated total reflection (ATR) module (Model-Alpha, Bruker, Germany). The infrared spectra was recorded at the frequency range of 4000–600 cm^{-1} with 32 consecutive scans at 1 cm^{-1} resolution. ^1H nuclear magnetic resonance (^1H NMR, Bruker DPX 500 MHz NMR spectrometer) spectra of EBHET-OH and pre-polymer was recorded at 500 MHz using deuterated acetone (C_2D_6O) as solvent and tetramethylsilane as internal reference. The ^1H NMR spectra of BHET was recorded at 300 MHz (Bruker) using deuterated chloroform ($CDCl_3$) as solvent and tetramethylsilane as reference. Differential scanning calorimetry (DSC, Mettler Toledo 822e) thermogram of BHET was recorded in the range of 40–200 °C at a heating rate of 10 °C/min using copper pan under nitrogen atmosphere. For polyester, the DSC was carried out from −70 °C to 200 °C under nitrogen atmosphere at a heating rate of 10 °C/min using DSC 200 F3 instrument (Netzsch, Germany). Thermo gravimetric analysis (TGA) was recorded using PerkinElmer, TGA 4000 instrument within the temperature range of 40–600 °C at a scan rate of 10 °C/min using alumina crucible under nitrogen atmosphere. X-ray diffraction (XRD) spectra was recorded by a wide angle X-ray scattering diffractometer (Panalytical) with Cu K_α radiation (1.544 Å) in the range of 5–80° (2θ) at 40 kV and 30 mA. The mechanical properties of the polyesters were carried out by using a universal testing machine (UTM) (Model-H5KT, Tinius Olsen, USA) equipped with data acquisition software at room temperature according to ASTM D638 standards at an elongation rate of 5 mm/min. The surface water wettability of the polyester was recorded by sessile drop technique with Theta QC, Biolin Scientific Finland.

The crosslinking density and molecular weight of polymer chain in between the crosslinks were calculated using the rubber elastic equation reported elsewhere [51].

$$n = \frac{E}{3RT} = \frac{\rho}{M_c}$$

where n is the number of active chain segment, per unit volume (mol/m^3), E is the Young's modulus in Pa, R is the universal gas constant 8.314 $m^3\,Pa\,K^{-1}\,mol^{-1}$, T is 37 °C (310°K) and ρ is the polymer density (gm/m^3) which was determined according to the previous report [51]. M_c is the molecular weight between crosslinks (gm/mole).

For swelling ratio measurement, post-polymers were cut into small pieces at the dimension of 10 × 10 × 2 $mm^3$and weighed (W_1) and immersed into double distilled water. After 1 day of swelling, the post-polymers were removed and weighed (W_2). The swelling ratio was calculated according to the following equation:

$$swelling\ ratio = \left(\frac{W_2 - W_1}{W_1}\right)$$

2.5. In-vitro degradation

For *in-vitro* degradation of the polyesters, the post-polymer samples were cut into a dimension of 10 × 10 × 2 $mm^3$and put in 25 ml phosphate buffer saline solution (PBS) having pH of 7.4. The whole degradation study was carried out under shaking condition (100 rpm) and at the temperature of 37 °C. PBS was changed at every 2 day of interval to avoid auto acceleration rate of hydrolysis. After regular intervals, the polymer films were removed from PBS and dried in a hot air oven at 55 °C until a steady weight was reached. All degradation experiments were carried out in triplicate. The degradation percentage was calculated using the following equation:

$$\%\ mass\ remaining = \frac{M_t}{M_0} \times 100$$

Here, M_t is the weight of polymer at different time intervals and M_0 is the initial weight of the polymer sample.

2.6. Fabrication of 3D scaffold

3D porous scaffold was fabricated by particulate leaching technique according to the previous study [55,56] with a newly developed technique. Briefly, the pre-polymer was dissolved in ethanol at a concentration of 0.25 g/ml. After that, the sieved sodium chloride having particle size within the range of 250–425 μm was taken into 2 ml polypropylene tube in such a manner that 2/3rd of the tube was filled (as shown in Fig. 6a). 1 ml of pre-polymer solution was added to the salt and mixed thoroughly by vortexing followed by centrifugation at 10,000 rpm for 10 min for close packing of the salt particles. The solvent was evaporated by placing the tubes in fume hood for 24 h and then kept at 120 °C for 5 day for post polymerization. After post polymerization, the tubes were cut into small pieces at a thickness of 5 mm with a sharp cutter. Subsequently, the small pieces were placed in excess double distilled water for 3 day with mild shaking to leach out the salts with changing the water at regular intervals. The 3D scaffolds were obtained after freeze drying (Hantech, South Korea) for 3 day followed by eliminating cautiously the plastic part outside the scaffold with the help of needle. The microstructure of 3D porous scaffolds was confirmed by field emission scanning electron microscopy (FESEM, JEOL JSM-7600F) after sputter coating with platinum for 10 min.

2.7. In-vitro mineralization on 3D scaffold in simulated body fluid (SBF)

SBF was prepared according to Kokubo et al. [57] in a scratch free empty cleaned plastic bottle. In details, 350 ml of ion exchanged distilled water was taken into the plastic bottle and stirred slowly at 37 °C. After that, 4.0175 g of sodium chloride (NaCl), 0.1775 g of sodium bicarbonate ($NaHCO_3$), 0.1125 g of potassium chloride (KCl), 0.1155 g of potassium hydrogen phosphate trihydrate ($K_2HPO_4{\cdot}3H_2O$), 0.1555 g of magnesium chloride hexahydrate ($MgCl_2{\cdot}6H_2O$), 1 (M) 19.5 ml of hydrochloric acid (HCl), 0.146 g of calcium chloride ($CaCl_2$) and 0.036 g of sodium sulphate (Na_2SO_4) were added one by one slowly (a regent was added after complete dissolution of preceding one). Finally, the rest of the ion exchanged distilled water was added to make the final volume of SBF to 500 ml.

For *in-vitro* mineralization, the scaffolds were immersed in SBF placed in a 24 well plate and incubated at 37 °C for 10 day. The SBF solution was changed at every 2 day of interval. After 10 day, the scaffolds were freeze dried after mild washing and characterized by XRD, FE-SEM and EDAX for the confirmation of mineral deposition.

2.8. Cell proliferation and viability assay

2.8.1. Cell culture

Mouse embryonic stem cell, OP9 (ATCC® USA CRL2749™) were used for cell culture study. The cells were cultured in DMEM supplemented with 20% (v/v) heat inactivated FBS and 1% penicillin–-streptomycin antibiotics. The cells were maintained at 37 °C and in CO_2 incubator under 5% CO_2 (ESCO Global). The cells were subcultured and used for experiment at 60–70% confluency.

2.8.2. Cell seeding on polymer film

Different composition of polyester films were cut into small pieces having dimension of 5 mm in diameter and 1 mm in thickness. All samples were sterilized by autoclave followed by ethanol treatment. After evaporation of ethanol in biosafety cabinet, the samples was washed with PBS for several times to remove any trace of ethanol. Finally, the samples were put in 96 well plate and incubated with

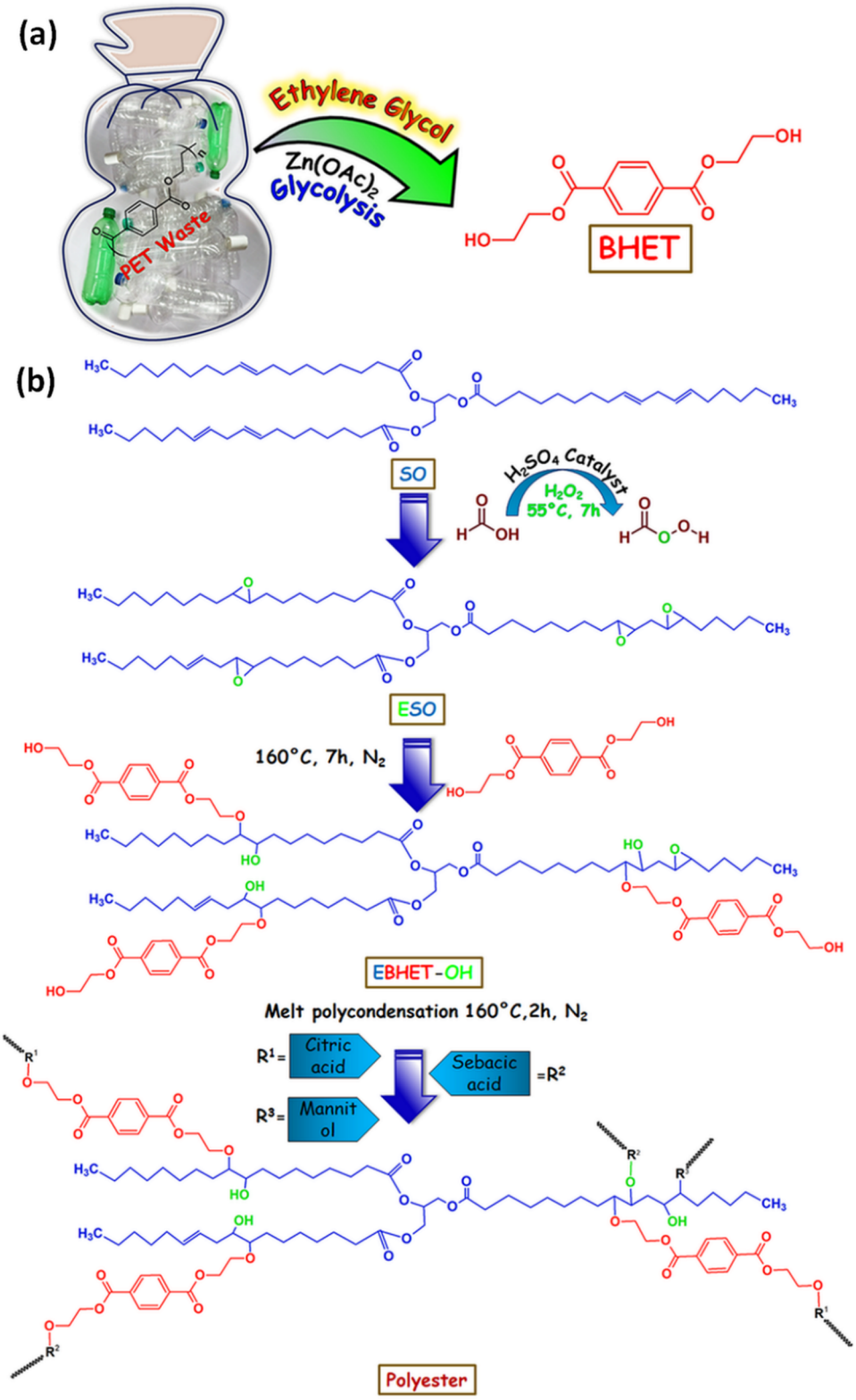

Fig. 1. Schematic representation for the synthesis of monomers such as BHET, ESO, EBHET-OH and the polyester.

culture medium for 24 h in CO_2 incubator to remove any unreacted monomers presented in post-polymer. After that, 2×10^3 cells were seeded on the polymer films and cultured in CO_2 incubator at 37 °C for 1, 4 and 7 day. To observe the cell attachment and cell proliferation, MTT assay was carried out at 1, 4 and 7 day.

2.8.3. MTT assay

Cell viability and proliferation on the polymer films were quantified by measuring the absorbance of formazan crystals at predetermined time intervals such as 1, 4 and 7 day. Before addition of MTT, the media was removed from each well and replaced with fresh DMEM media containing 10 µl of MTT solution (5 mg/ml) in each well of 96 well plate. After that, the plate was incubated for 4 h at 37 °C followed by

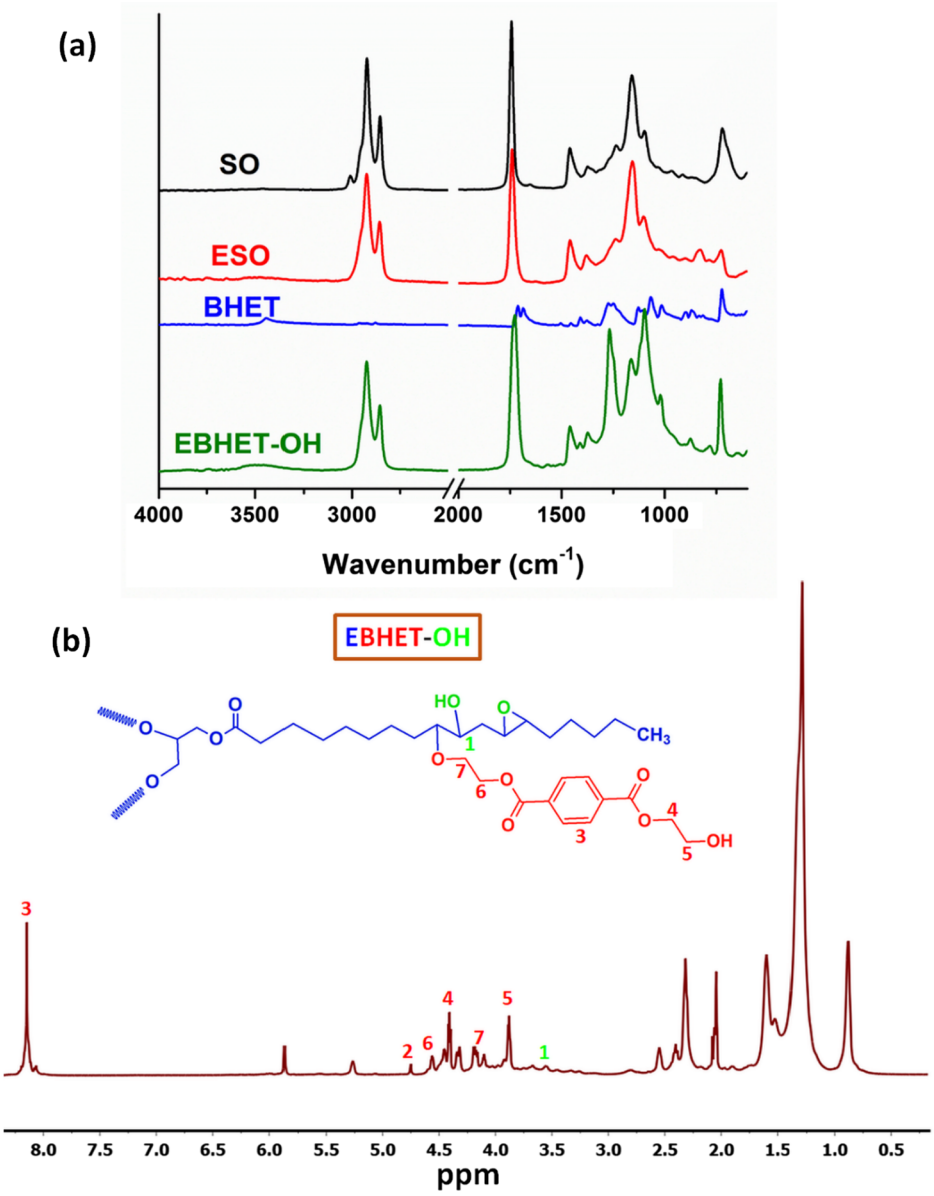

Fig. 2. FTIR spectra of SO, ESO, BHET, EBHET-OH (a), NMR spectra of EBHET-OH (b).

removal of the media and addition of 100 µl of DMSO to dissolve the formazan crystals formed by the live cell. After complete dissolution of formazan crystals, polymer films were taken out from DMSO and consequently the absorbance was recorded at 578 nm by plate reader (Erba LisaScan EM, Transasia). All experiments was performed in triplicate. All data were represented in triplicates (± SD).

2.8.4. Alizarin Red-S assay

To confirm the bone mineralization through osteogenic differentiation of stem cell, we carried out Alizarin Red-S (ARS) straining. After predetermined time intervals such as 7 and 14 day, attached cells on the films were fixed with 4% paraformaldehyde for 30 min at 37 °C followed by staining with ARS (10 mg/ml) for 30 min after washing with PBS thrice. After that, films were rinsed several times with double distilled water to remove excess amount of dye and dried by ethanol gradient. Digital images of stained films were collected by a digital camera. To quantify the stained dye, stained films were immersed in 200 µl of 0.5 (N) HCl containing 5% SDS for 30 min to dissolve the dye and subsequently the absorbance of the dissolved dye was measured at 405 nm using plate reader. All experiments were performed in triplicate.

2.8.5. Alcian blue assay

To check the chrondogenesis of stem cells, Alcian Blue (AB) assay was performed. Similar to ARS straining, AB staining was carried out after fixation of the attached cells on the films by 4% paraformaldehyde for 30 min at 37 °C followed by staining with AB dye for 30 min. Digital images of stained films were captured by a digital camera after removing unstained dye with washing several times with double distilled water followed by drying with ethanol gradient. After dissolving the stained AB dye in 200 µl of 6(M) guanidine hydrochloride solution for overnight, the absorbance of the dissolved AB dye was recorded at 630 nm using plate reader. All experiments were carried out in triplicate.

2.9. Statistical analysis

All the UTM, degradation and biological experiments were conducted in triplicate for reproducibility and the data are presented here in the form of average value ± the standard deviation (SD). Two-way

ANOVA in Graphpad Prism software was used to for statistical analysis and for *, ** and *** were considered for p values < 0.05, < 0.01 and < 0.001 respectively.

3. Results and discussion

3.1. Polyester synthesis

Despite the development of several biopolymers for tissue engineering application, suitable and inexpensive biopolymer is still remained undiscovered for interfacial tissue regeneration. Most of the biopolymers either useful for bone regeneration or cartilage formation. Primarily this is due to complex material composition and mechanical properties, it is difficult to regenerate tissue interface such as bone-cartilage using a single biopolymer. The existing biopolymers have limited clinical application for tissue regeneration due to its huge production cost. In this context, biopolymers derived from waste material or renewable resources may solve this problem for this life saving emerging field. Being inspired from our previous studies [50,51], we hypothesized that the incorporation of soybean oil through epoxidation into BHET, SA, CA and MA based polyester may develop a novel low cost biopolymer for tissue engineering application. The presence of aromatic ring in BHET and the long aliphatic hydrocarbon chain in soybean oil may provide hard segment and soft segment, respectively which consequently may form tissue interface such as bone-cartilage for ITE application. Prior to the synthesis of polyester, the polyol (EBHET-OH) was synthesized by the reaction of ESO and BHET through solvent and catalyst free ring opening reaction as shown in Fig. 1. Consequently, the polyester was synthesized by melt polycondensation reaction between the EBHET-OH and dicarboxylic acid (SA) in presence of CA and MA which acted as crosslinker. All polyesters synthesized by catalyst and solvent free melt condensation process to minimize any unwanted cytotoxicity which is prime parameter for biomedical applications. All polyesters were consisted of two step processes including pre-polymerization followed by post-polymerization. Pre-polymerization is 2 h reaction where a waxy like polymer is obtained and completely cured polyester is formed after post-polymerization for 5 day at 120 °C. A series of polyesters were synthesized here just varying the composition of ESO and BHET during the synthesis of EBHET-OH and keeping constant the ratio of EBHET-OH: SA: CA: MA at 2: 1: 1: 0.5.

3.2. Structural characterization

The synthesis of starting materials such as BHET, ESO and EBHET-OH was characterized by FTIR and ^{1}H NMR as shown in Fig. 2. Fig. 2a shows the characteristic peaks of SO at 3008 cm^{-1} due to the trans C—H stretching of —CH=CH—, the peak at 2923 and 2854 cm^{-1} corresponding to the asymmetric and symmetric stretching of $-CH_2$ and at 1744 cm^{-1} related to the C=O stretching of triglyceride groups. After epoxidation of SO, the peak at 3008 cm^{-1} completely disappeared and a new peak appeared at 827 cm^{-1} corresponding to the epoxide group which indicates the conversion of double bonds to epoxide ring as reported previously [51]. On the other hand, the presence of sharp peak at 3442 cm^{-1} (—OH stretching), less intense peak at 1713 cm^{-1} (C=O stretching of ester group) and sharp peak at 723 cm^{-1} (para substituted aromatic ring) signify the synthesis of BHET from recycled PET through glycolysis as evidenced by Sarkar et al. [50] The synthesis of BHET from PET was further confirmed by ^{1}H NMR, DSC, TGA and XRD as shown in Figs. S1 and S2. DSC spectra (Fig. S2b) shows the melting point of BHET is 114 °C which is well correlated with the previous report [50]. Fig. S2 represents XRD patterns of PET having a broad peak at 25°.But, BHET obtained by depolymerization of PET shows sharp peaks due to its crystalline nature. The major peaks are observed at 7°, 16.7°, 21.3°, 23.6° and 27.8° which are almost similar to as reported by Zhou et al. [58] After the ring opening reaction of ESO by BHET, the appearance of broad stretching peak at 3479 cm^{-1}, strong bending peak at 1100 cm^{-1} corresponding to the hydrogen bonded —OH group, sharp $-CH_2$ stretching peak at 2924 and 2854 cm^{-1} as well as the disappearance of epoxide peak at 825 cm^{-1} confirm the synthesis of EBHET-OH. In addition to this, the change of ester peak position of BHET or ESO from 1713 or 1739 cm^{-1}, respectively to 1727 cm^{-1} for EBHET-OH also suggests the formation of a new compound after reaction of ESO and BHET which attributes the synthesis of EBHET-OH.

The synthesis of polyol was further confirmed by ^{1}H NMR and the corresponding NMR spectra are represented in Fig. 2b. Usually epoxidized soybean oil demonstrates three significant peaks in between 2.8 and 3.3 ppm [51,59]. Whereas these peaks are completely disappeared after ring opening reaction of ESO by BHET and new peak observed at 8.2 ppm corresponding to the aromatic ring present in polyol. Additionally, appearance of more new peaks at 4.6 ppm (2H at number 6, red), 4.4 ppm (2H at number 4, red), 4.1 ppm (2H at number 7, red) and 3.8 ppm (2H at number 5, red) further confirms the synthesis of EBHET-OH through ring opening reaction of ESO by BHET. These data confirms the synthesis of staring materials such as BHET and EBHET-OH successfully.

The synthesis of polyester was also characterized by FTIR, ^{1}H NMR, XRD and TGA and the corresponding spectra are shown in Fig. 3. Fig. 3a shows the FTIR spectra of post-polymerized polyesters with varying ESO: BHET ratios of 3:1, 4:1, 5:1 and 6:1. It is observed that with increasing the ESO content the peak intensity at 1708 cm^{-1} corresponding to C=O stretching of ester group gradually decreased. The reason can be explained that with increasing ESO content (i.e. decreasing BHET content) the number of —OH groups in polyol (EBHET-OH) gradually decreased and consequently formation of ester groups (through reaction of polyol and dicarboxylic acid such as SA) also decreased which resulted in gradual decrease of C=O stretching peak intensity as observed in Fig. 3a. A broad peak at 3491 cm^{-1} was observed for the polyester having ESO-BHET weight ratio of 3:1 indicating the presence of unreacted hydrogen bonded —OH groups in the polyester. As the number of —OH groups decreased with increasing the ESO:BHET weight ratio and the number of available —OH groups in the polyol (EBHET-OH) completely participated in the polycondensation reaction for esterification which showed complete disappearance of the —OH stretching peak at 3500 cm^{-1} region as shown in Fig. 3a for the polyesters having ESO:BHET weight ratios of 4:1, 5:1 and 6:1. These data suggests the synthesis of polyesters.

To validate the FTIR data, we further carried out ^{1}H NMR of synthesized polyester and the corresponding ^{1}H NMR spectra of pre-polymer (as the post-polymer is insoluble in any solvent) having ESO:BHET weight ratio of 4:1 is shown in Fig. 3b. Due to complex structure of the polymer and overlapping of the peaks, the ^{1}H NMR spectra in Fig. 3b suggests the presence of all monomers in the pre-polymer. The peaks in between 4.0 and 4.5 ppm and at 8.2 ppm confirms the presence of BHET in the polyester. The two peaks at 1.3 and 2.3 ppm also suggest the presence of SA in the polymer backbone while the peaks in between 2.7 and 3.0 ppm are corresponding to CA and MA.

The extent of crystallinity of the polyesters after post-polymerization was analyzed by XRD analysis and the corresponding spectra are shown in Fig. 3c. From Fig. 3c, it is observed that the polyester shows typical characteristic crystalline peak at 19.3° (2θ) along with amorphous peak at 41° (2θ). Similar type of crystalline peak of BHET based polyester was also obtained in the previous report [50]. It is also notices that the intensity of crystalline peak initially increased from ESO:BHET weight ratio from 3:1 to 4:1 and then declined with further increasing the ESO:BHET weight ratio. As discussed in Fig. 3a, there was incomplete reaction at the ESO:BHET weight ratio of 3:1 whereas complete esterification reaction occurred at the weight ratio of 4:1 and consequently resulted increased crystalline peak intensity compared to that of the weight ratio of 3:1. The crystallinity may be obtained due to presence of aromatic ring in the polyester backbone. Due to further increment of ESO content (lowering BHET content) beyond the ESO:BHET weight ratio of 4:1, the amorphous content in the polyester

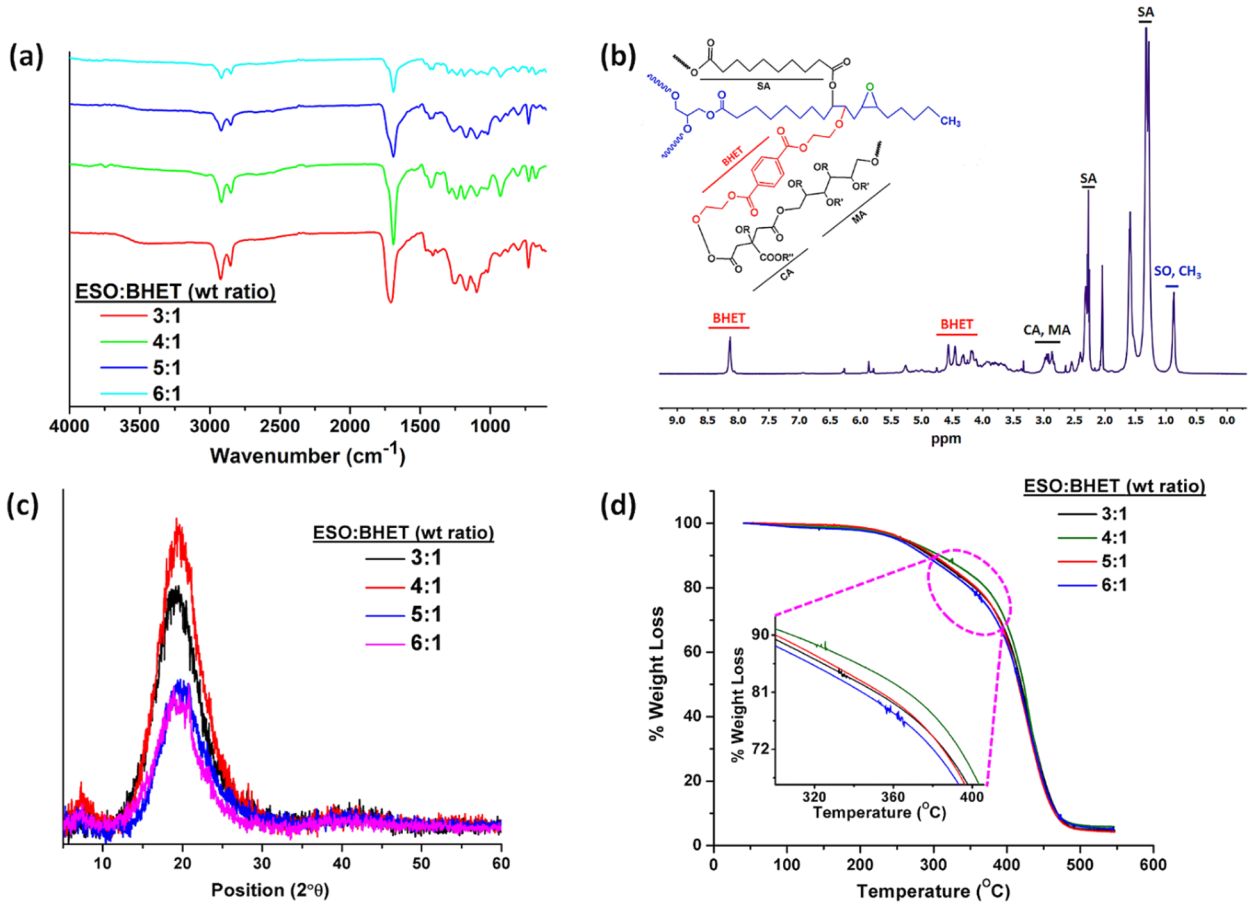

Fig. 3. FTIR of the post-polymer polyester with the ESO:BHET weight ratios of 3:1, 4:1, 5:1 and 6:1 (a), ^{1}H NMR spectra of pre-polymer polyester with the ESO:BHET weight ratio of 4:1 (b), XRD spectra (c) and TGA spectra (d) of the post-polymer polyester with the ESO:BHET weight ratios of 3:1, 4:1, 5:1.

increased which resulted the reduction of crystalline peak intensity at the ESO:BHET weight ratio of 5:1 and 6:1.

The post-polymers are also thermally well stable which was characterized by TGA and the corresponding thermogram spectra are shown in Fig. 3d. Fig. 3d shows that the polyesters are thermally stable up to 225 °C without any significant weight loss. However, all polyesters showed very slow degradation beyond the temperature of 225 °C and around 25% weight loss occurred at the temperature of 225 °C. After that temperature a sharp weight loss happened at the temperature of 430 °C (obtained from derivative curve, Fig. S3) and complete thermal degradation of all polyesters occurred at the temperature of around 480 °C. However, among the different polyesters, the polyester comprises with ESO:BHET weight ratio of 4:1 showed comparatively better thermal stability (shown in inset) which may be due to the presence of more crystallinity in its structure as shown in XRD (Fig. 3c). Due to presence of lowest crystalline region in the polyester of ESO:BHET ratio of 6:1 (as observed in XRD analysis), it showed comparatively lowest thermal stability.

To know more information like glass transition temperature (T_g) about the polymer, we further performed differential scanning calorimetry (DSC) and the respective DSC thermograms and calculated T_g of the polyesters at different ESO:BHET ratios are shown in Fig. 4. Fig. 4a depicts the respective DSC curves of the post–polymerized polyesters at different ESO:BHET weight ratios. Fig. 4a does not show any melting peaks which suggests the elastomeric nature of the synthesized polyesters. Previous report also supports this observation [51]. Generally elastomer shows single T_g below room temperature but thermoplastic elastomer exhibits two different T_g due to presence of elastomeric soft segment and thermoplastic hard segment. Interestingly, here two or more T_g are observed for the elastomeric polyesters at various ESO:BHET weight ratios as shown in Table 1.

Two, one, one and three T_g were obtained for ESO:BHET weight ratio of 3:1, 4:1, 5:1 and 6:1, respectively from DSC thermogram (calculated from instrument software). We further calculated the respective T_g by second derivatives of DSC thermograms and the corresponding second derivative graph is shown in Fig. 4b. It is found that the T_g values calculated from second derivative graph and instrument software were almost same as given in Table 1. The polyester having ESO:BHET weight ratio of 3:1 showed two T_g at −24.3 °C (-25.1 °C, instrument data) and 15.6 °C (21.4 °C, instrument data) which may be due to the presence of soft segment (attributed by long alkyl chain of ESO part) and hard segment (attributed by BHET part), respectively as shown schematically in Fig. 4c. As discussed in the previous section (Fig. 3a), the unreacted ESO-BHET polyol completely reacted in the polyester of 4:1 ESO:BHET weight ratio and comparatively higher crystallinity (as shown in Fig. 3c) of the polyester might show a single T_g (−4.6 °C) which is in between the T_g of the polyester of 3:1 ESO:BHET weight ratio. In 4:1 ESO:BHET weight ratio polyester, the hard segment predominated the amorphous soft segment (shown in Fig. 4c) and the overall elastomeric nature of the polyester might show less negative T_g compared to 3:1 ESO:BHET weight ratio polyester. With further increasing the ESO content in the polyester with ESO:BHET weight ratio of 5:1, the quantity of amorphous soft segment increased (also reflected in XRD spectra, Fig. 3c) and consequently lowered the T_g value (−17.9 °C, Fig. 4b) compared to that of preceding polyester (4:1 ESO:BHET weight ratio). Interestingly, the polyester with ESO:BHET weight ratio of 6:1 showed three T_g having the values of −24.2, 1.4 and 17.2 °C which may be corresponding to the soft segment (attributed by long alkyl chain of ESO), hard segment (attributed by BHET) and self-induced crystalline hard segment (as shown by dotted

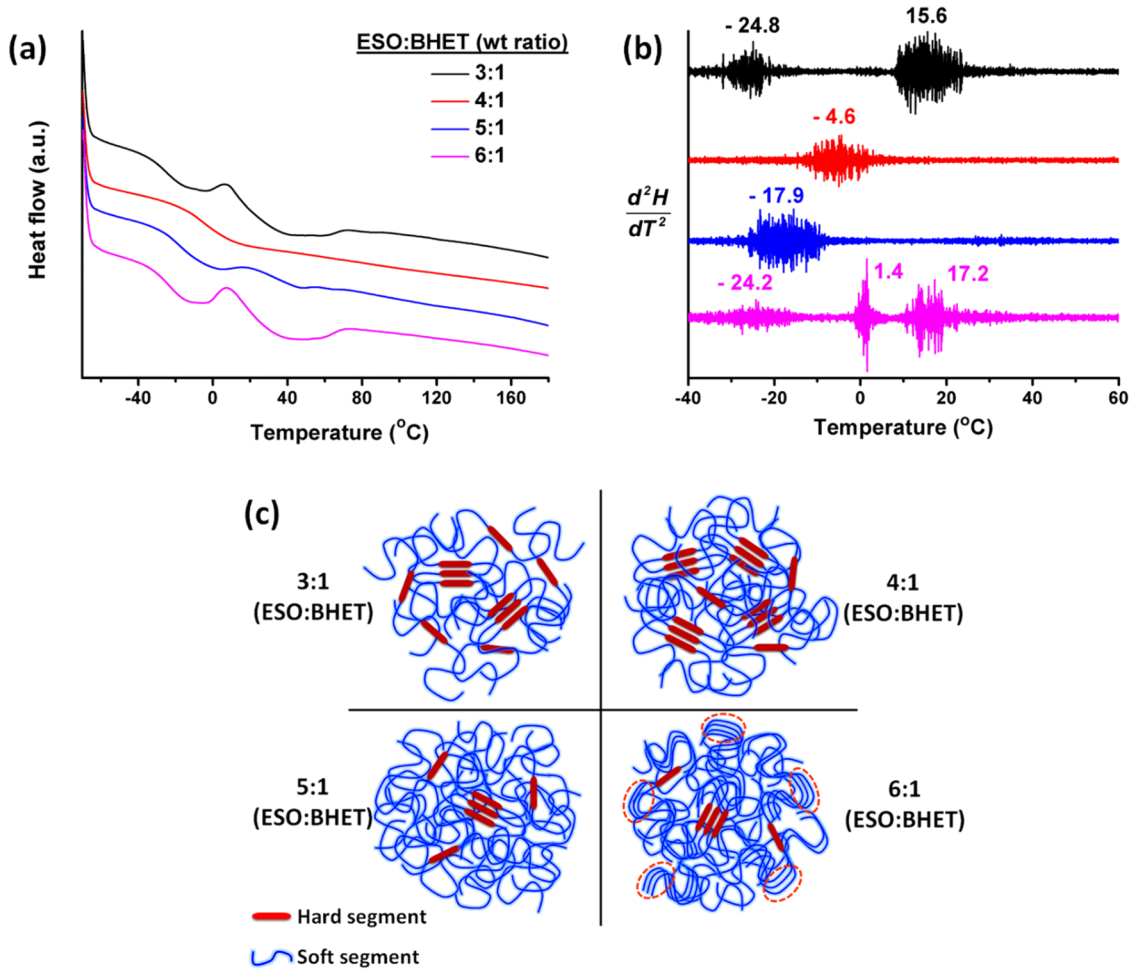

Fig. 4. DSC spectra of post-polymer polyester with the ESO:BHET weight ratios of 3:1, 4:1, 5:1 and 6:1 (a) and their corresponding second order derivative curves (b), schematic representation for the hypothesis of polymer chain conformation which is responsible for different T_g of the polyester (c).

Table 1
Comparative T_g values of different post-polymers determined from instrument software and 2nd derivative of DSC thermograms.

Sample ESO:BHET (weight ratio)	T_g measured by instrument software (°C)			T_g measured by second derivative of DSC thermograms (°C)		
	T_{g1}	T_{g2}	T_{g3}	T_{g1}	T_{g2}	T_{g3}
3:1	−25.1	21.4	–	−24.8	15.6	–
4:1	−4.1	–	–	−4.6	–	–
5:1	−16.2	–	–	−17.9	–	–
6:1	−24.6	21.1	1.7	−24.2	17.2	1.4

circle in Fig. 4c, below right of fourth quadrant), respectively.

3.3. Mechanical properties

In addition to the thermal properties of any newly developed polymer, it is also necessary to know about its mechanical properties of that polymer. Respective tensile stress-strain curve, ultimate tensile strength, Young's modulus and elongation at break of the post-polymerized polyesters at various ESO:BHET weight ratios are shown in Fig. 5. Fig. 5a represents typical stress-strain curve of the polyesters at different ESO:BHET weight ratios of 3:1, 4:1, 5:1 and 6:1. Stress-strain curve shows the elastomeric nature for all polyesters. Polyester having ESO:BHET weight ratio of 3:1 shows intermediate mechanical properties with Young's modulus, ultimate tensile strength and elongation at break of 1.91 ± 0.44 MPa (Fig. 5b), 0.21 ± 0.04 MPa (Fig. 5c) and 84 ± 22% (Fig. 5d), respectively. Due to the superior crystallinity of the polyester with 4:1 ESO:BHET weight ratio (as discussed in previous section, Fig. 3c), the mechanical properties significantly increased compared to all polyesters and the corresponding Young's modulus, and ultimate tensile strength are 3.64 ± 0.26 MPa (Fig. 5b), 0.34 ± 0.08 MPa (Fig. 5c), respectively and consequently its elongation at break decreased from 84 ± 22% to 62 ± 10% (Fig. 5d). With further increasing the ESO:BHET weight ratio (ESO:BHET weight ratio 5:1), the elongation at break significantly increased from 62 ± 10% to 184 ± 5% (Fig. 5d) which results the suppression of mechanical properties and the corresponding Young's modulus and ultimate tensile strength are 0.66 ± 0.07 MPa and 0.12 ± 0.03 MPa, respectively. This was occurred due to the decreasing of crystallinity of the polyester with increasing the ESO content as shown in Fig. 3c. Interestingly, the Young's modulus and ultimate tensile strength of the polyester with ESO:BHET weight ratio of 6:1 increased compared to that of 5:1 ESO:BHET weight ratio polyester despite the presence of higher amount of ESO content and lowest crystallinity (as shown in Fig. 3c). This phenomenon may be due to the formation of self-induced crystalline domains by the alkyl chain of ESO as shown schematically in Fig. 4c and consequently resulted the augmentation of Young's modulus and ultimate tensile strength with the value of 2.03 ± 0.63 MPa (Fig. 5b) and 0.19 ± 0.03 MPa (Fig. 5c), respectively. As expected, the elongation at break of the polyester decreased from 184 ± 5% to 62 ± 6% (Fig. 5d). The elastic modulus of these polyesters closely similar to human tissues such as soft collagenous bone, ligaments etc.

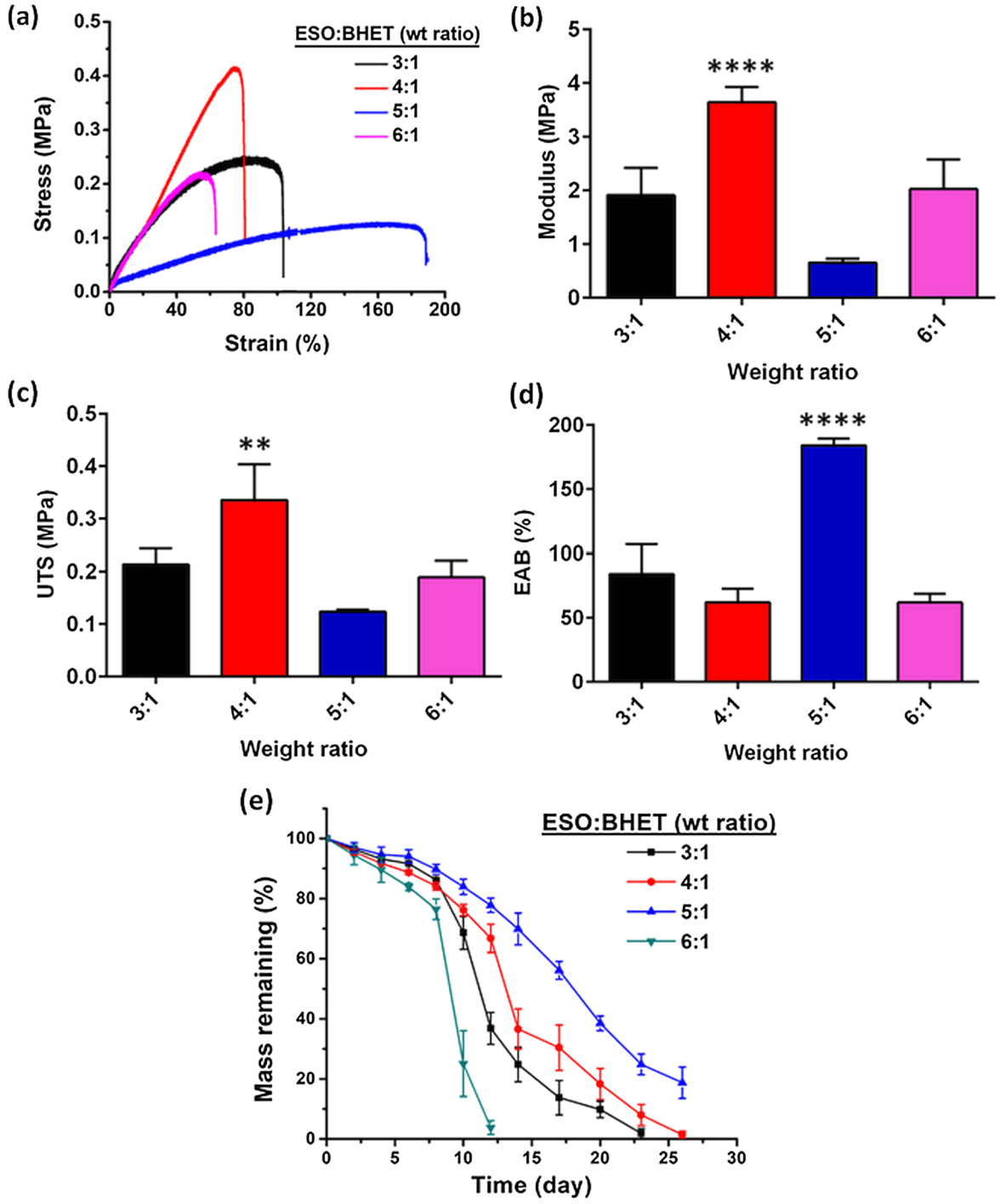

Fig. 5. Typical stress-strain curves (a), calculated Young's modulus (b), ultimate tensile strength (c) and elongation at break of the post-polymer polyester with the ESO:BHET weight ratios of 3:1, 4:1, 5:1 and 6:1 (d). *In-vitro* degradation data of post-polymer polyester with the ESO:BHET weight ratios of 3:1, 4:1, 5:1 and 6:1 in PBS buffer (e).

3.4. In vitro degradation

For successful tissue engineering application, the polymeric biomaterial should be biodegrable within a particular time period. Despite the presence of enormous suitable properties of various biopolymers such as polycaprolactone (PCL), poly-l-lactic acid (PLA), poly(glycolic acid) (PGA) etc. for tissue engineering application, poor and slow degradation rate limits its clinical application for tissue regeneration. Therefore, we checked the *in vitro* hydrolytic degradation of the synthesized polyesters in PBS buffer at 37 °C prior to the further biological studies for tissue regeneration and the corresponding degradation profile is shown in Fig. 5e. It is observed that all polyesters at different ESO:BHET weight ratios degraded completely within a month. Among the all polyesters, the polyester having ESO:BHET weight ratio of 6:1 showed fast degradation rate, $k_d = 2.80 \times 10^{-3}\, g/h$ (shown in Table 2) and completely degraded within 15 days. The poor crystallinity (as shown in Fig. 3c) may facilitated to penetrate more water molecules inside the polymeric architecture (evident by highest swelling ratio with the value of 3.80, Table 2) and resulted fast degradation through bulk erosion as reported in previous report [Sarkar et al.]. Due to more

Table 2
Comparative values of crosslinking density, molecular weights between two crosslinking units, swelling ratio, degradation rate constant and contact angle of different post-polymers.

Sample ESO:BHET (wt ratio)	Crosslinking density (mol/m^3)	Molecular weight between cross-links (M_c) (g/mol)	Swelling ratio	Degradation rate constant (k_d) (g/h) ($\times 10^{-3}$)	Contact angle (Degree)
3:1	247 ± 56	4244	1.80	2.04	99.0 ± 0.5
4:1	470 ± 34	2299	0.06	1.19	88.1 ± 0.4
5:1	85 ± 9	11,412	0.08	0.71	92.2 ± 0.4
6:1	262 ± 82	3814	3.80	2.80	93.7 ± 0.1

elastomeric nature of the polyester having ESO:BHET weight ratio of 5:1 may be attributed to slowest degradation rate ($k_d = 0.71 \times 10^{-3}\, g/h$, Table 2) and ~80% degradation occurred after 30 days (as shown in Fig. 5e). The polyesters with ESO:BHET weight ratios of 4:1 and 3:1 showed moderate degradation rates with the values of $k_d = 1.19 \times 10^{-3}\, g/h$ and $k_d = 2.04 \times 10^{-3}\, g/h$, respectively. The molecular weight of the polymer also played an important role on degradation rate. From Table 2 it is noticed that the polyester of 5:1 ESO:BHET weight ratio possessed highest molecular weight segments ($M_c = 11,412\, g/mol$, Table 2) in between the two crosslinking sites which resulted slowest degradation rate among the all polyesters. Not only molecular weight of polymer segment in between two crosslinking site but also crosslinking densities have a combined effect on the degradation rate. By the combination of molecular weight and crosslinking density, the degradation rate of the polyesters followed the order $k_{d\,(6:1)} < k_{d\,(3:1)} < k_{d\,(4:1)} < k_{d\,(5:1)}$.

3.5. Fabrication of 3D-scaffold

3D scaffolds were initially prepared by salt leaching method according to the previous reported techniques such as compression technique [55] and 96 well plate technique [56]. Unfortunately, porous 3D scaffold was not formed using this polymer as shown in Fig. 6b (compression technique) and c (96 well plate technique). In the previous work, the authors used PCL as the polymeric material and obtained 3D porous scaffold through dissolving PCL in chloroform followed by mixing with sodium chloride salt, making disk by compression or putting in 96 well plate and then evaporating the solvent and finally leaching out the salt and lyophilization. Here, the polymer system is different and the final usable polymer is obtained after post-polymerization preceding by pre-polymerization. After following previous reported methods, we had to post-polymerize after evaporating the solvent and got 3D scaffold with distorted surface without any pore after leaching out of salt particles and lyophilization (Fig. 6b and c). This phenomenon may be explained by the fact that during post-polymerization the polymer flows slightly which might form a polymer skin over the salt particle and results closed pore after leaching out of the salt particle. For successful tissue regeneration, the scaffold should have interconnected porous structure which facilitates cell growth, proliferation and differentiation [14,18]. To overcome this problem, we developed a new method for fabrication of 3D porous scaffold as described in previous section and shown schematically in Fig. 6a. The corresponding SEM images of the 3D scaffold obtained from the polyester with ESO:BHET weight ratio of 4:1 are shown in Fig. 6d (low magnification) and e (high magnification). Fig. 6d shows nicely 3D porous interconnected structure with the pore size within the range of 250–450 μm without formation of any polymer skin as obtained in previous reported methods (Fig. 6b and c). The high magnification image (Fig. 6e) shows micropores within the macropore (shown by white arrow) which may facilitate the nutrient transportation for better cell growth. Therefore, this technique may be an attractive way to fabricate the 3D porous scaffold for this type of polymer system.

3.6. In-vitro mineralization in SBF

As the composition of SBF is almost similar to the human blood plasma [60], the suitability of any biomaterial to form bone in *in vivo* model can be assessed by the formation of apatite on the surface of the biomaterial in SBF. Therefore, we carried out *in vitro* mineralization study on the 3D scaffold of the polyester with ESO:BHET weight ratio of 4:1 in SBF. The apatite formation on the scaffold was confirmed by FESEM, EDAX and XRD and the corresponding images and spectra are shown in Fig. 7. Fig. 7a and b depict the typical FESEM images of 3D porous scaffold before and after immersing in SBF, respectively. Fig. 7a shows nice porous architecture of the polyester 3D scaffold (ESO:BHET weight ratio of 4:1) with the pore size within the range of 250–450 μm which is ideal for bone formation [61] before mineral deposition in SBF. Surprisingly, the pore size significantly decreased through mineral deposition after 10 days of incubation in SBF and the pore size becomes to around 10–100 μm as shown in Fig. 7b. The appearance of calcium (Ca) and phosphorus (P) peak at 2.2 and 3.8 keV, respectively in EDAX spectra (Fig. 7d) after 10 days of incubation in SBF confirms the mineral deposition of the 3D scaffold. The deposition of hydroxyl apatite, which is main component for bone was further confirmed by XRD and the related XRD spectra are shown in Fig. 7e. Fig. 7e shows the XRD graph of pure hydroxyapatite which shows the typical peaks at 31.7, 32.1 and 32.8° for 211, 112 and 300 plane, respectively. These data are well correlated to the JCPDS (09-0432) of hydroxyapatite. After 10 day of incubation in SBF, 3D scaffold showed the appearance of new peak within the range of 31–33° confirms the deposition of hydroxyapatite on the scaffold. Therefore, the polyester scaffold would be suitable for bone formation in *in vivo*.

3.7. Cytocompatibility assay

Prior to the bio-application of any new material, it is necessary to check the cytocompatibility of that material. Here, we used polyester 2D film with various ESO:BHET weight ratios for all biological studies. For cytocompatibility assay of the polyester 2D films, MTT assay was carried out at different intervals such as 1, 4 and 7 day and the corresponding data is shown in Fig. 8a. From Fig. 8a, it is observed that almost same number of cells were attached on the polyester 2D films with all ESO:BHET weight ratios compared to control TCPS plate after 1 day of cell seeding which suggests the cytocompatibility of the polyester at all ESO:BHET weight ratios. The contact angle values of the polyester surface at all ESO:BHET weight ratios lie within the value of 88–99° (shown in Table 2) which are moderate values for cell attachment as supported the previous report [51,62]. The number of cells did not change after 4 day of culture for the polyester 2D films with ESO:BHET weight ratios of 3:1 and 4:1 which are comparatively hard polyester. But the cell number significantly increased (comparable or better than control TCPS surface) on the comparatively soft polyester films with ESO:BHET weight ratios of 5:1 and 6:1 after 4 day of incubation. Surprisingly, the cell number dramatically increased especially on 3:1 and 4:1 ESO:BHET weight ratio containing polyester film after 14 day of culture. Although, the polyester with 5:1 ESO:BHET weight ratio showed better cell proliferation among the all polyester

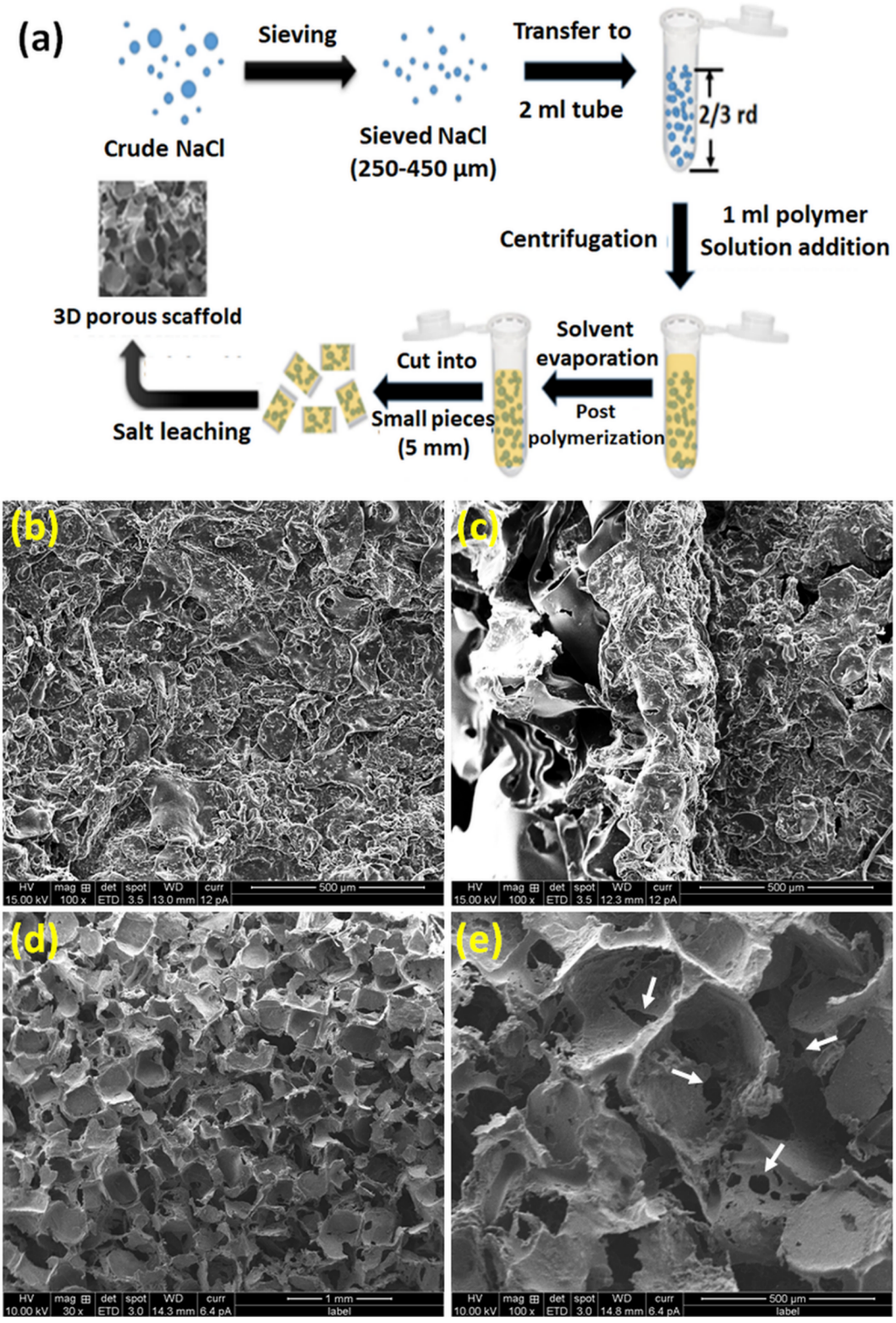

Fig. 6. Schematic representation for the fabrication of 3D scaffold by salt leaching method (a). SEM image of 3D scaffold obtained from post-polymer polyester with ESO:BHET weight ratio of 4:1 by compression technique (b), 96 well plate technique (c) and low magnification image (d) and high magnification image (e) of newly developed technique in this work.

films and even control TCPS surface. There is a strong correlation between the cell attachment and its proliferation with mechanical properties of the polymer [63]. Li et al. [64] observed that the number of cell attachment after 1 day of seeding on the material surface decreased with increasing the material hardness or elastic modulus. Cell proliferation also decreased with increasing material hardness and they obtained maximum cell proliferation on comparatively soft surface after 5 day of culture. Similarly, Murikipudi et al. [65] reported on how the substrate modulus effects on the cell number and its growth rate. They also noticed that the cell numbers significantly increased on soft

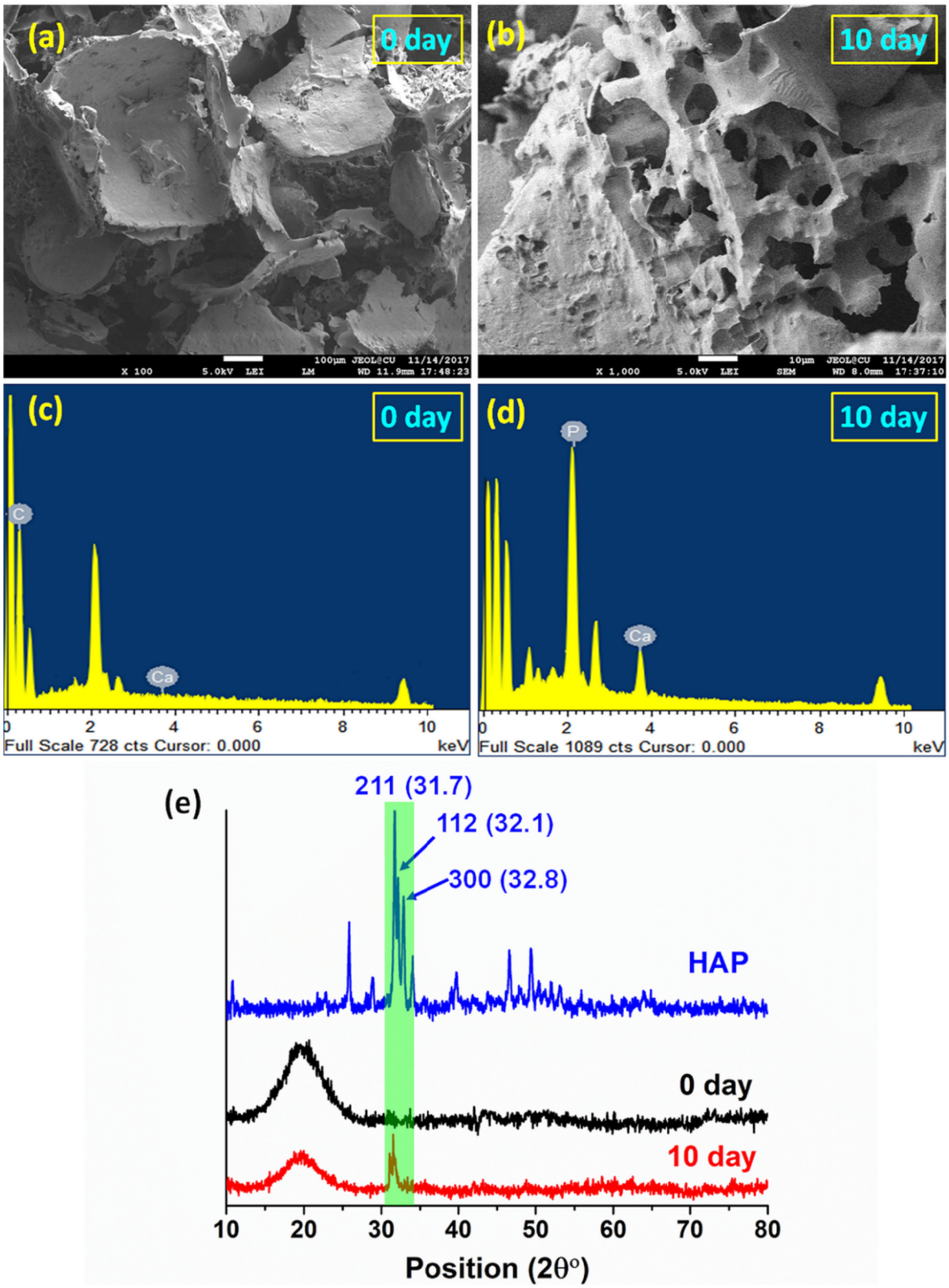

Fig. 7. SEM images of *in vitro* mineralized 3D scaffold of polyester having ESO:BHET weight ratio of 4:1 in SBF at 0 day (a) and 10 day (b). The corresponding EDAX spectra of the mineralized 3D scaffold at 0 day (c) and 10 day (d). XRD spectra of the mineralized 3D scaffold of polyester having ESO:BHET weight ratio of 4:1 at 0 and 10 day of incubation in SBF along with hydroxyapatite (e).

polymeric scaffold having modulus of 0.5 kPa whereas least number of cells was obtained on highest modulus (1.4 kPa) scaffold after 21 day of culture. Cell proliferation or growth rate also followed similar trend as cell number. Here, we also observed similar trend where comparatively soft polyester (ESO:BHET weight ratio of 5:1) facilitated better cell attachment and cell proliferation compared to that of hard polyester. The result suggests the cytocompatibility of the polyesters at all ESO:BHET weight ratios.

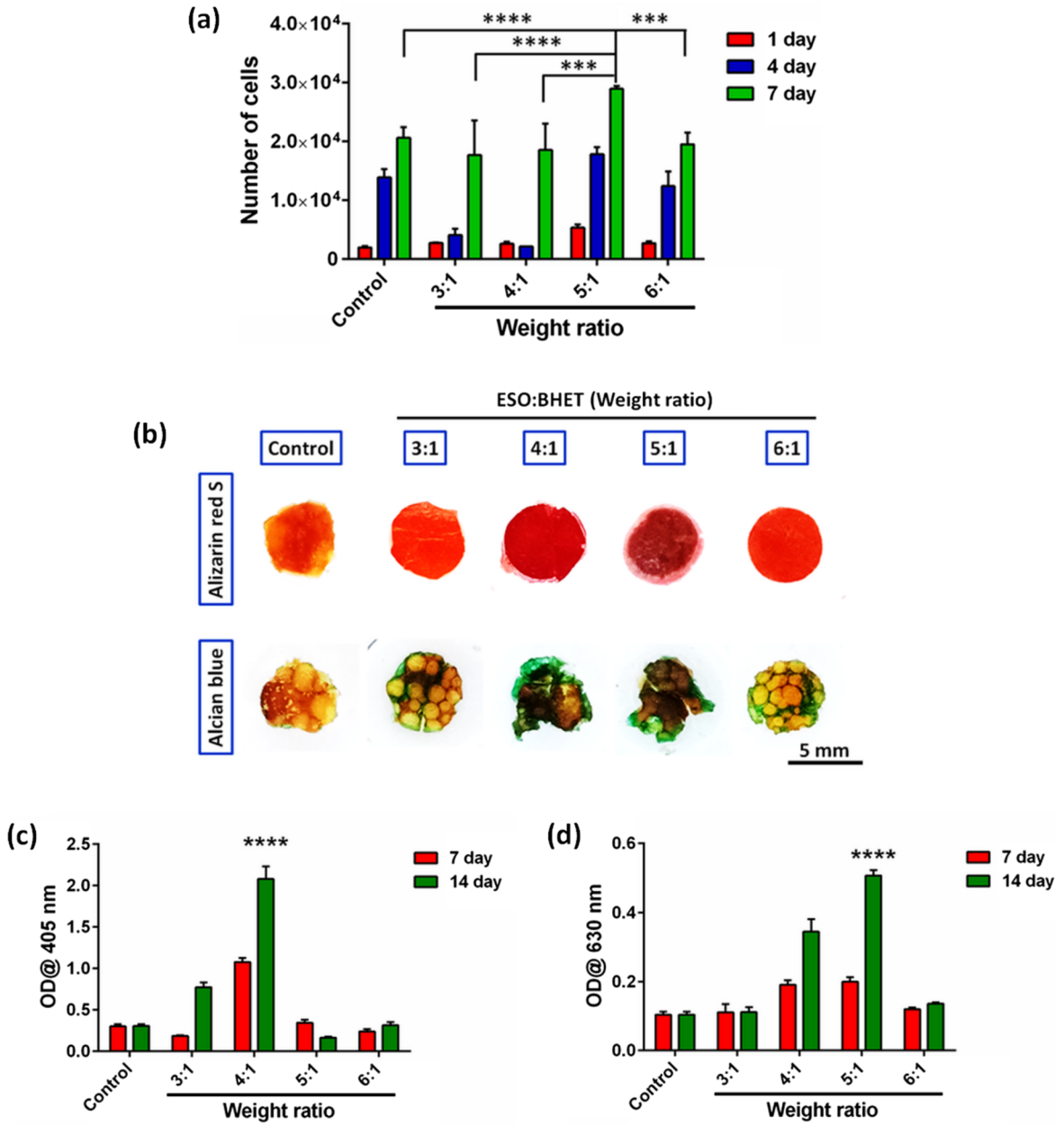

Fig. 8. *In vitro* cell viability of 2D post-polymer polyester films having ESO:BHET weight ratios of 3:1, 4:1, 5:1 and 6:1 towards mouse embryonic stem cell (OP9) at various time intervals of 1 day, 4 day and 7 day (a). Digital pictures of stained polyester 2D films by alizarin-red S (for bone formation) and alcian blue (for cartilage formation) through osteogenic and chondrogenic differentiation, respectively of stem cells (b) and the corresponding quantification of alizarin red (c) and alcian blue (d) after 7 and 14 day cell culture.

3.8. Osteogenic and chondrogenic differentiation

In OA patients, the articular cartilage and the underlying subchondral bone become damaged. Currently, there are no existing therapeutic treatment to cure or regenerate such type of osteochondral defect. Despite the enormous advancement in tissue engineering field, conventional tissue engineering fails to regenerate such osteochondral tissue interface due to presence of complex mechanical properties and material composition. Interfacial tissue engineering has shown some hope for the regeneration of osteochondral tissue interface [33,34,36–38]. As per hypothesis of this work, we seeded the mouse embryotic stem cells on 2D polyester films with all ESO:BHET weight ratios and cultured for 7 and 14 days followed by staining with alizarin red and alcian blue to confirm the osteogenesis and chondrogenesis of stem cell, respectively. The corresponding photographic images of the stained 2D polyester films are shown in Fig. 8b. Alizarin red generally forms complex with calcium and results red color whereas alcian blue complexes with proteoglycan present in collagen to form cyan color. Fig. 8b shows that the red color intensity gradually increased with increasing the ESO:BHET weight ratio and maximum color intensity was obtained for ESO:BHET weight ratio of 4:1 and then the color intensity declined beyond the ESO:BHET weight ratio of 4:1. As the polyester 2D film itself has slightly reddish brown color, so we quantified the color intensity through dissolving the alizarin red-Ca complex in HCl and SDS solution mixture followed by measuring the OD and the corresponding data are represented in Fig. 8c. The polyester with ESO:BHET weight ratio of 4:1 showed highest OD value after 7 and 14 day which signifies the formation of highest quantity of calcium through osteogensis of stem cell. With further increasing of ESO:BHET weight ratio (ESO:BHET weight ratio of 5:1 and 6:1), the OD value significantly decreased. The

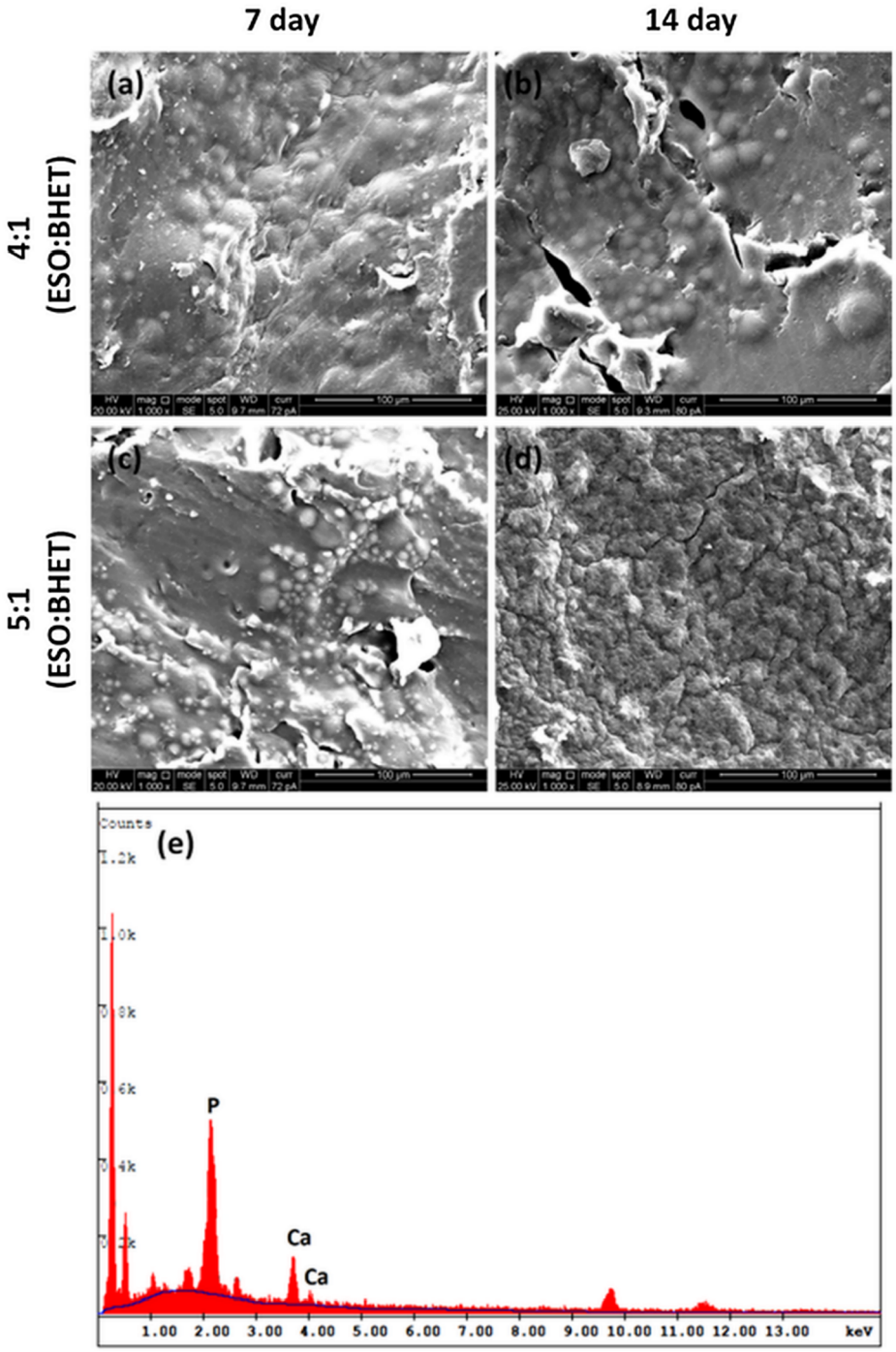

Fig. 9. SEM images of 2D post-polymer polyester films with ESO:BHET weight ratio of 4:1 (a, b) and 5:1 (c, d) after 7 and 14 day of cell culture. The corresponding EDAX spectra of 2D post-polymer films ESO:BHET weight ratio of 4:1 after 14 day of cell culture (e).

superior Young's modulus (3.64 ± 0.26 MPa) and tensile strength (0.34 ± 0.08 MPa) of the polyester with ESO:BHET weight ratio of 4:1 might guide the stem cell towards osteogenesis. Similar effect was found in previous studies [66–68].

In addition to this, the presence of aromatic moiety (from BHET part) in the polyester architecture might also help in osteoconduction for osteogenesis of stem cell and resulted the formation of more bone mineral i.e. calcium. With increasing the ESO:BHET weight ratio, the content of BHET decreased which reduces the osteoconductivity and subsequently less calcium was formed through stem cell osteogenesis.

On the other hand, the polyesters with ESO:BHET weight ratios of 4:1 and 5:1 showed almost similar color intensity (Fig. 8b, here it is looking bottle green which is obtained by combining cyan color with the polyester reddish brown color) after staining with alcian blue which attributes the formation of similar amount of collagen through chondrogenesis of stem cell. The quantification data (Fig. 8d) shows that both the polyesters with ESO:BHET weight ratios of 4:1 and 5:1 showed similar OD values after 7 day but the OD value significantly increased for the polyester with ESO:BHET weight ratio of 5:1 after 14 day which signifies the formation of more collagen through chondrogenesis of stem cell. The lowest mechanical properties (Young's modulus and ultimate tensile strength are 0.66 ± 0.07 MPa and 0.12 ± 0.03 MPa, respectively) for the polyester with ESO:BHET weight ratio of 5:1 might guide the stem cell towards the chondrogenic differentiation as

observed in previous report [66–68]. It is noticed that the polyester with ESO:BHET weight ratio of 4:1 promotes both the bone formation as well as cartilage formation compared to all other polyesters. Not only the mechanical cues of the polyester stimulated the stem cell differentiation but also the degraded product from the polyester might promote the stem cell differentiation towards both osteogenic and chondrogenic differentiation as found in previous report [69,70]. The formation of bone minerals was further confirmed by SEM and EDAX and the corresponding SEM images and EDAX spectra are shown in Fig. 9. From SEM images it is observed that the stem cell became round shaped after both 7 and 14 day of culture on the polyester 2D film having ESO:BHET weight ratio of 4:1 as shown in Fig. 9a and b, respectively. Whereas some cells acquired round shaped morphology after 7 day of culture (Fig. 9c) but the overall round shaped morphology disappeared after 14 day (Fig. 9d) on the polyester 2D film with ESO:BHET weight ratio of 5:1. EDAX spectra of Fig. 9b shows the presence of calcium (3.8 keV) and phosphorous (2.1 keV) which further supports the formation of bone minerals through osteogenesis of stem cell on the polyester with ESO:BHET weight ratio of 4:1.

4. Conclusion

A family of low cost biodegradable and biocompatible polyesters were synthesized using SO, BHET (derived from recycled PET waste) and other low cost, renewable resources such as SA, CA and MA by eco-friendly, catalyst free and solvent free melt polycondensation process. The mechanical properties and degradation rates of the polyesters can be fine-tuned by varying the weight ratio of ESO and BHET. Deposition of hydroxyapatite on the 3D scaffold in SBF suggests that the polyester is suitable for bone tissue engineering application. Attachments and proliferation of mouse embryotic stem cells on the 2D polymer films suggest that polyesters are cytocompatible. The mechanical cues of the polyesters guided the stem cell towards osteogenic and chondrogenic differentiation although the differentiation was dependent on ESO:BHET weight ratios in the polyester. Among the different polyesters, the polyester with the ESO:BHET weight ratio of 4:1 showed both osteogenesis along with the chondrogenesis. Therefore, the polyester with the ESO:BHET weight ratio may be regenerate osteo-chondral tissue interface which is essential for OA patients although animal studies are required before that.

Declaration of Competing Interest

The authors declare no conflicts of interest.

Acknowledgements

This work is financially supported by DST-SERB funding agency through two sanctioned projects EEQ/2016/000712 and ECR/2016/002018. K.S. also acknowledge UGC for UGC-BSR Research Start-Up Grant (F.30-363/2017(BSR), Dt- 08/08/2017) and CU for UPE-II Nanofabrication project fund (UGC/166/UPE-II, Dt- 03/04/2017) for financial support. KG and KS also acknowledge Mr. Purusottom Das for NMR characterization. KG and KS also thankful to Professor Sukumar Roy and Professor Amit Roy Chowdhury for mechanical testing of the polymer samples.

Appendix A. Supplementary material

Supplementary data to this article can be found online at https://doi.org/10.1016/j.eurpolymj.2019.109338.

References

[1] D.J. Hunter, D. Schofield, E. Callander, The individual and socioeconomic impact of osteoarthritis, Nat. Rev. Rheumatol. 10 (7) (2014) 437.
[2] T. Vos, R.M. Barber, B. Bell, A. Bertozzi-Villa, S. Biryukov, I. Bolliger, F. Charlson, A. Davis, L. Degenhardt, D. Dicker, Global, regional, and national incidence, prevalence, and years lived with disability for 301 acute and chronic diseases and injuries in 188 countries, 1990–2013: a systematic analysis for the Global Burden of Disease Study 2013, The Lancet 386 (9995) (2015) 743–800.
[3] L. Hangody, G. Kish, Z. Karpati, I. Szerb, I. Udvarhelyi, Arthroscopic autogenous osteochondral mosaicplasty for the treatment of femoral condylar articular defects A preliminary report, Knee Surg. Sports Traumatol. Arthrosc. 5 (4) (1997) 262–267.
[4] A. Carranza-Bencano, L. García-Paino, J.A. Padron, A.C. Dominguez, Neochondrogenesis in repair of full-thickness articular cartilage defects using free autogenous periosteal grafts in the rabbit. A follow-up in six months, Osteoarthritis cartilage 8 (5) (2000) 351–358.
[5] S.L. Sledge, Microfracture techniques in the treatment of osteochondral injuries, Clin. Sports Med. 20 (2) (2001) 365–378.
[6] P. Livesley, M. Doherty, M. Needoff, A. Moulton, Arthroscopic lavage of osteoarthritic knees, The Journal of bone and joint surgery, British 73 (6) (1991) 922–926.
[7] K. Ghosal, R. Khanna, K. Sarkar, Biopolymer Based Interfacial Tissue Engineering for Arthritis, in: B. Li, T. Webster (Eds.), Orthopedic Biomaterials : Progress in Biology, Manufacturing, and Industry Perspectives, Springer International Publishing, Cham, 2018, pp. 67–88.
[8] J. Paul, A. Sagstetter, M. Kriner, A. Imhoff, J. Spang, S. Hinterwimmer, Donor-site morbidity after osteochondral autologous transplantation for lesions of the talus, JBJS 91 (7) (2009) 1683–1688.
[9] L. Hangody, J. Dobos, E. Baló, G. Pánics, L.R. Hangody, I. Berkes, Clinical experiences with autologous osteochondral mosaicplasty in an athletic population: a 17-year prospective multicenter study, Am. J. Sports Med. 38 (6) (2010) 1125–1133.
[10] F.P. Luyten, J. Vanlauwe, Tissue engineering approaches for osteoarthritis, Bone 51 (2) (2012) 289–296.
[11] M.E. Gomes, M.T. Rodrigues, R.M. Domingues, R.L. Reis, Tissue engineering and regenerative medicine: new trends and directions—a year in review, Tissue Eng. Part B: Rev. 23 (3) (2017) 211–224.
[12] C. Mandrycky, K. Phong, Y. Zheng, Tissue engineering toward organ-specific regeneration and disease modeling, MRS Commun. 7 (3) (2017) 332–347.
[13] L.G. Zhang, A. Khademhosseini, T. Webster, Tissue and Organ Regeneration: Advances in Micro-and Nanotechnology, CRC Press, 2016.
[14] F.J. O'Brien, Biomaterials & scaffolds for tissue engineering, Mater. Today 14 (3) (2011) 88–95.
[15] S. Sundelacruz, D.L. Kaplan, Stem cell- and scaffold-based tissue engineering approaches to osteochondral regenerative medicine, Semin. Cell Dev. Biol. 20 (6) (2009) 646–655.
[16] K. Lee, E.A. Silva, D.J. Mooney, Growth factor delivery-based tissue engineering: general approaches and a review of recent developments, J. R. Soc. Interface 8 (55) (2011) 153–170.
[17] K. Ghosal, K. Sarkar, Biomedical applications of graphene nanomaterials and beyond, ACS Biomater. Sci. Eng. 4 (8) (2018) 2653–2703.
[18] R. Langer, Biomaterials in drug delivery and tissue engineering: one laboratory's experience, Acc. Chem. Res. 33 (2) (2000) 94–101.
[19] P.J. Yang, J.S. Temenoff, Engineering orthopedic tissue interfaces, Tissue Eng. Part B: Rev. 15 (2) (2009) 127–141.
[20] M.M. Stevens, Biomaterials for bone tissue engineering, Mater. Today 11 (5) (2008) 18–25.
[21] R. Stoop, Smart biomaterials for tissue engineering of cartilage, Injury 39 (1) (2008) 77–87.
[22] S. Sambit, C.-H. James Goh, S.-L. Toh, Development of hybrid polymer scaffolds for potential applications in ligament and tendon tissue engineering, Biomed. Mater. 2(3) (2007) 169.
[23] K.-H. Jeong, D. Park, Y.-C. Lee, Polymer-based hydrogel scaffolds for skin tissue engineering applications: a mini-review, J. Polym. Res. 24 (7) (2017) 112.
[24] M. Singh, N. Dormer, J.R. Salash, J.M. Christian, D.S. Moore, C. Berkland, M.S. Detamore, Three-dimensional macroscopic scaffolds with a gradient in stiffness for functional regeneration of interfacial tissues, J. Biomed. Mater. Res. Part A 94A (3) (2010) 870–876.
[25] L. Liverani, A.R. Boccaccini, 6 - Multilayered scaffolds for interface tissue engineering applications A2 - Guarino, Vincenzo, in: L. Ambrosio (Ed.), Electrofluidodynamic Technologies (EFDTs) for Biomaterials and Medical Devices, Woodhead Publishing, 2018, pp. 107–122.
[26] M. Ramalingam, M.F. Young, V. Thomas, L. Sun, L.C. Chow, C.K. Tison, K. Chatterjee, W.C. Miles, C.G. Simon, Nanofiber scaffold gradients for interfacial tissue engineering, J. Biomater. Appl. 27 (6) (2013) 695–705.
[27] G. Criscenti, A. Longoni, A.D. Luca, C.D. Maria, C.A.V. Blitterswijk, G. Vozzi, L. Moroni, Triphasic scaffolds for the regeneration of the bone–ligament interface, Biofabrication 8 (1) (2016).
[28] K. Sajedeh, K. Akbar, A review on gradient hydrogel/fiber scaffolds for osteochondral regeneration, J. Tissue Eng. Regener. Med. 12 (4) (2018) e1974–e1990.
[29] L. Paul, T. Katelyn, C. Wei, F. Ya-Lin, Z. Gan, J. Radoslaw, N.B. Shelke, X. Yu, S.G. Kumbar, Bioactive polymeric scaffolds for osteochondral tissue engineering: in vitro evaluation of the effect of culture media on bone marrow stromal cells, Polym. Adv. Technol. 26 (12) (2015) 1476–1485.
[30] N.H. Dormer, M. Singh, L. Wang, C.J. Berkland, M.S. Detamore, Osteochondral interface tissue engineering using macroscopic gradients of bioactive signals, Ann. Biomed. Eng. 38 (6) (2010) 2167–2182.
[31] G. Criscenti, A. Longoni, A. Di Luca, C. De Maria, C. Van Blitterswijk, G. Vozzi, L. Moroni, Triphasic scaffolds for the regeneration of the bone–ligament interface, Biofabrication 8 (1) (2016) 015009.
[32] N. Mohan, N.H. Dormer, K.L. Caldwell, V.H. Key, C.J. Berkland, M.S. Detamore,

Continuous gradients of material composition and growth factors for effective regeneration of the osteochondral interface, Tissue Eng. Part A 17 (21–22) (2011) 2845–2855.
[33] X. Shao, J.C. Goh, D.W. Hutmacher, E.H. Lee, G. Zigang, Repair of large articular osteochondral defects using hybrid scaffolds and bone marrow-derived mesenchymal stem cells in a rabbit model, Tissue Eng. 12 (6) (2006) 1539–1551.
[34] W. Zhang, Q. Lian, D. Li, K. Wang, D. Hao, W. Bian, J. He, Z. Jin, Cartilage repair and subchondral bone migration using 3D printing osteochondral composites: a one-year-period study in rabbit trochlea, Biomed Res. Int. 2014 (2014).
[35] J. Chen, H. Chen, P. Li, H. Diao, S. Zhu, L. Dong, R. Wang, T. Guo, J. Zhao, J. Zhang, Simultaneous regeneration of articular cartilage and subchondral bone in vivo using MSCs induced by a spatially controlled gene delivery system in bilayered integrated scaffolds, Biomaterials 32 (21) (2011) 4793–4805.
[36] J. Liao, T. Tian, S. Shi, X. Xie, Q. Ma, G. Li, Y. Lin, The fabrication of biomimetic biphasic CAN-PAC hydrogel with a seamless interfacial layer applied in osteochondral defect repair, Bone Res. 5 (2017) 17018.
[37] S. Saha, B. Kundu, J. Kirkham, D. Wood, S.C. Kundu, X.B. Yang, Osteochondral tissue engineering in vivo: a comparative study using layered silk fibroin scaffolds from mulberry and nonmulberry silkworms, PLoS ONE 8 (11) (2013) e80004.
[38] Z. Ting, Z. Hefeng, Z. Laquan, J. Shuaijun, L. Jian, X. Zhuo, S. Wei, Biomimetic design and fabrication of multilayered osteochondral scaffolds by low-temperature deposition manufacturing and thermal-induced phase-separation techniques, Biofabrication 9 (2) (2017) 025021.
[39] T.J. Levingstone, A. Ramesh, R.T. Brady, P.A. Brama, C. Kearney, J.P. Gleeson, F.J. O'Brien, Cell-free multi-layered collagen-based scaffolds demonstrate layer specific regeneration of functional osteochondral tissue in caprine joints, Biomaterials 87 (2016) 69–81.
[40] X. Wang, E. Wenk, X. Zhang, L. Meinel, G. Vunjak-Novakovic, D.L. Kaplan, Growth factor gradients via microsphere delivery in biopolymer scaffolds for osteochondral tissue engineering, J. Control. Release 134 (2) (2009) 81–90.
[41] L. Andrea Di, L. Alessia, C. Giuseppe, L.-M. Ivan, K.-G. Michel, V. Julius, B. Clemens van, M. Carlos, M. Lorenzo, Surface energy and stiffness discrete gradients in additive manufactured scaffolds for osteochondral regeneration, Biofabrication 8 (1) (2016) 015014.
[42] A. Di Luca, B. Ostrowska, I. Lorenzo-Moldero, A. Lepedda, W. Swieszkowski, C. Van Blitterswijk, L. Moroni, Gradients in pore size enhance the osteogenic differentiation of human mesenchymal stromal cells in three-dimensional scaffolds, Sci. Rep. 6 (2016) 22898.
[43] S. Chaudhary, P. Surekha, D. Kumar, C. Rajagopal, P.K. Roy, Microwave assisted glycolysis of poly (ethylene terepthalate) for preparation of polyester polyols, J. Appl. Polym. Sci. 129 (5) (2013) 2779–2788.
[44] I. Vitkauskienė, R. Makuška, Glycolysis of industrial poly (ethylene terephthalate) waste directed to bis (hydroxyethylene) terephthalate and aromatic polyester polyols, Chemija 19 (2) (2008).
[45] G.P. Karayannidis, A.K. Nikolaidis, I.D. Sideridou, D.N. Bikiaris, D.S. Achilias, Chemical recycling of PET by glycolysis: polymerization and characterization of the dimethacrylated glycolysate, Macromol. Mater. Eng. 291 (11) (2006) 1338–1347.
[46] C.N. Hoang, Y.H. Dang, Aminolysis of poly (ethylene terephthalate) waste with ethylenediamine and characterization of α, ω-diamine products, Polym. Degrad. Stab. 98 (3) (2013) 697–708.
[47] K. Ghosal, K. Sarkar, Poly(ester amide) derived from municipal polyethylene terephthalate waste guided stem cells for osteogenesis, New J. Chem. 43 (35) (2019) 14166–14178.
[48] H. Kurokawa, M.-A. Ohshima, K. Sugiyama, H. Miura, Methanolysis of polyethylene terephthalate (PET) in the presence of aluminium tiisopropoxide catalyst to form dimethyl terephthalate and ethylene glycol, Polym. Degrad. Stab. 79 (3) (2003) 529–533.
[49] D. Carta, G. Cao, C. D'Angeli, Chemical recycling of poly (ethylene terephthalate) (PET) by hydrolysis and glycolysis, Environ. Sci. Pollut. Res. 10 (6) (2003) 390–394.
[50] K. Sarkar, S.R.K. Meka, A. Bagchi, N. Krishna, S. Ramachandra, G. Madras, K. Chatterjee, Polyester derived from recycled poly (ethylene terephthalate) waste for regenerative medicine, RSC Adv. 4 (102) (2014) 58805–58815.
[51] E. Kolanthai, K. Sarkar, S.R.K. Meka, G. Madras, K. Chatterjee, Copolyesters from soybean oil for use as resorbable biomaterials, ACS Sustain. Chem. Eng. 3 (5) (2015) 880–891.
[52] D.G. Barrett, M.N. Yousaf, Design and applications of biodegradable polyester tissue scaffolds based on endogenous monomers found in human metabolism, Molecules 14 (10) (2009) 4022–4050.
[53] M. Reinecker, V. Soprunyuk, M. Fally, A. Sánchez-Ferrer, W. Schranz, Two glass transitions of polyurea networks: Effect of the segmental molecular weight, Soft Matter 10 (31) (2014) 5729–5738.
[54] R.T. Tran, L. Wang, C. Zhang, M. Huang, W. Tang, C. Zhang, Z. Zhang, D. Jin, B. Banik, J.L. Brown, Synthesis and characterization of biomimetic citrate-based biodegradable composites, J. Biomed. Mater. Res. Part A 102 (8) (2014) 2521–2532.
[55] G. Kumar, C.K. Tison, K. Chatterjee, P.S. Pine, J.H. McDaniel, M.L. Salit, M.F. Young, C.G. Simon, The determination of stem cell fate by 3D scaffold structures through the control of cell shape, Biomaterials 32 (35) (2011) 9188–9196.
[56] G.M. Balachander, S.A. Balaji, A. Rangarajan, K. Chatterjee, Enhanced Metastatic Potential in a 3D Tissue Scaffold toward a Comprehensive in Vitro Model for Breast Cancer Metastasis, ACS Appl. Mater. Interfaces 7 (50) (2015) 27810–27822.
[57] T. Kokubo, H. Takadama, How useful is SBF in predicting in vivo bone bioactivity? Biomaterials 27 (15) (2006) 2907–2915.
[58] X. Zhou, X. Lu, Q. Wang, M. Zhu, Z. Li, Effective catalysis of poly(ethylene terephthalate) (PET) degradation by metallic acetate ionic liquids, Pure Appl. Chem. (2012) 789.
[59] J. Natarajan, Q. Dasgupta, S.N. Shetty, K. Sarkar, G. Madras, K. Chatterjee, Poly (ester amide)s from Soybean Oil for Modulated Release and Bone Regeneration, ACS Appl. Mater. Interfaces 8 (38) (2016) 25170–25184.
[60] T. Kokubo, Bioactive glass ceramics: properties and applications, Biomaterials 12 (2) (1991) 155–163.
[61] L.A. Cyster, D.M. Grant, S.M. Howdle, F.R.A.J. Rose, D.J. Irvine, D. Freeman, C.A. Scotchford, K.M. Shakesheff, The influence of dispersant concentration on the pore morphology of hydroxyapatite ceramics for bone tissue engineering, Biomaterials 26 (7) (2005) 697–702.
[62] D.P. Dowling, I.S. Miller, M. Ardhaoui, W.M. Gallagher, Effect of Surface Wettability and Topography on the Adhesion of Osteosarcoma Cells on Plasma-modified Polystyrene, J. Biomater. Appl. 26 (3) (2011) 327–347.
[63] S. Ali, I.B. Wall, C. Mason, A.E. Pelling, F.S. Veraitch, The effect of Young's modulus on the neuronal differentiation of mouse embryonic stem cells, Acta Biomater. 25 (2015) 253–267.
[64] J. Li, X. Wang, Y. Lin, X. Deng, M. Li, C. Nan, In vitro cell proliferation and mechanical behaviors observed in porous zirconia ceramics, Materials (Basel, Switzerland) 9 (4) (2016) 218.
[65] S. Murikipudi, H. Methe, E.R. Edelman, The effect of substrate modulus on the growth and function of matrix-embedded endothelial cells, Biomaterials 34 (3) (2013) 677–684.
[66] A.J. Engler, S. Sen, H.L. Sweeney, D.E. Discher, Matrix elasticity directs stem cell lineage specification, Cell 126 (4) (2006) 677–689.
[67] A.S. Mao, J.-W. Shin, D.J. Mooney, Effects of substrate stiffness and cell-cell contact on mesenchymal stem cell differentiation, Biomaterials 98 (2016) 184–191.
[68] O.F. Zouani, J. Kalisky, E. Ibarboure, M.-C. Durrieu, Effect of BMP-2 from matrices of different stiffnesses for the modulation of stem cell fate, Biomaterials 34 (9) (2013) 2157–2166.
[69] V.S. Sukanya, P.V. Mohanan, Degradation of Poly(ε-caprolactone) and bio-interactions with mouse bone marrow mesenchymal stem cells, Colloids Surf. B: Biointerfaces 163 (2018) 107–118.
[70] C. Gao, S. Peng, P. Feng, C. Shuai, Bone biomaterials and interactions with stem cells, Bone Res. 5 (2017) 17059.